A HIRES ANALYSIS OF THE FIR EMISSION OF SUPERNOVA REMNANTS

ZHONG WANG
Infrared Processing and Analysis Center, MS 100-22,
California Institute of Technology, Jet Propulsion Laboratory,
Pasadena, CA 91125

ABSTRACT The HiRes algorithm has been used to analyze the far-infrared emission of shocked gas and dust in supernova remnants. In the case of supernova remnant IC 443, we find a very good match between the resolved features in the deconvolved images and the emissions of shocked gas mapped in other wavelengths (lines of H_2, CO, HCO+, and HI). Dust emission is also found to be surrounding hot bubbles of supernova remnants which are seen in soft X-ray maps. Optical spectroscopy on the emission of the shocked gas suggests a close correlation between the FIR color and local shock speed, which is a strong function of the ambient (preshock) gas density. These provide a potentially effective way to identify regions of strong shock interaction, and thus facilitate studies of kinematics and energetics in the interstellar medium.

INTRODUCTION

Supernova remnants (SNRs) can be bright in the mid- and far-infrared either because of non-thermal radiative processes internally, or interactions with the interstellar medium (ISM) surrounding them. Several recent studies have surveyed a large number of Galactic SNRs in the IRAS All Sky Survey, and identified a substantial fraction of them as FIR sources despite considerable confusion problems due to the Galactic plane (Arendt 1989; Saken et. al. 1992). General correlations between IR and radio, and/or between IR and X-ray emissions are cited, even though the resolution that IRAS data provide is often insufficient to study the IR morphology. In addition, it is found on a statistical basis that older remnants are both colder and more massive. These results suggest that the emission measured by IRAS come mostly from shock interactions with dense gas and dust. However, the actual mechanism of interaction, and its dependence on local conditions largely remain to be explored.

An alternative approach to the statistical analysis is trying to better resolve the IR emission around a few extended SNRs, and compare the images in the four IRAS bands with the physical conditions in the surrounding medium studied in other wavelengths. In this way, one can hopefully address the origin of the infrared emission as well as the energy balance in the evolution of the remnants. The HiRes algorithm (Aumann et. al. 1990) becomes particularly useful in this regard, because it provides not only a much better linear resolution, but also a convenient way to examine infrared color variation through *beam matching*.

S. Terebey and J. Mazzarella (eds.), *Science with High-Spatial Resolution Far Infrared Data*, 157–163, 1994, Jet Propulsion Laboratory, Pasadena, CA.

In this contribution, I present the preliminary results of a HiRes analysis to illustrate some of the possibilities that this approach can provide.

DATA ANALYSIS

The FIR emission of supernova remnant IC 443 is detected in all four IRAS bands and its ring-like structure has been well identified (Huang et. al. 1986; Braun & Strom 1986; Arendt 1989). However, since the angular scale of the entire region is about 20′, the $\sim 4'$ resolution of the coadded images is inadequate to analyze the infrared morphology. As a result, only the integrated fluxes have been measured in the previous studies.

Since both the absolute flux level and the signal-to-nise ratio in the 60 and 100 μm images of SNRs are higher than that in 12 and 25 μm, it is justified to perform more HiRes iterations on the longer wavelength images. In practice, I used the survey data as input, and adopted the HiRes 12, 25, 60 and 100 μm images at 5, 5, 10, and 20 iterations, respectively. Although these do not provide the best possible resolution at all four bands, they do give more comparable beam sizes. More importantly, they are physically meaningful because of the different signal-to-noise ratios in the four bands. The region selected to perform the deconvolution is a 2° field centered on IC 443.

The variation of the beam from the field center to the sides is rather small in this case, so I adopted measurements of simulated beam at the image center to be the representative one. The next step was to examine the resolution maps at each band, and try to match the resolution based on the "least common denominator". Four different two-dimensional smoothing kernels were used to *convolve* the maps into nearly identical beam sizes and shapes, while preserving the best possible resolution. The parameters of the kernel used, and the measurements of input and output beams are listed in Table 1. These measurements were based on 2-D least-square Gaussian fits.

Table 1. Beam measurements[a]

	Before Convolution[b]		Gaussian Kernel[c]		After Convolution[b]	
Band(i)[d]	a(maj)	a(min)	*sa*	*ar*	a(maj)	a(min)
b1(5)	6.58	2.11	1.65	0.920	7.55	4.45
b2(5)	7.16	2.22	1.62	0.573	7.56	4.45
b3(10)	5.34	3.12	2.25	0.589	7.54	4.45
b4(20)	5.33	3.97	2.25	0.367	7.55	4.46

[a] all measurements are in unit of pixel, 1 pixel = 15″;
[b] a(maj), a(min) are half width along the major and minor axes, respectively;
[c] *sa*, *ar* are the semi-major axis and axis ratio of the 2-D Gaussian;
[d] bn(i): where n represents band id, and i is the number of iterations used.

From Table 1, we see that the beams in the four IRAS bands are well matched after convolution with the selected kernel, with a relatively minor penalty of a $\sim$ 30% increase in beamwidth. The beam matching of the actual images was confirmed by comparing a few stellar sources present in the same field. Figure 1 compares the *beam-matched* 60 and 100 μm images with the unprocessed ones. The resolution of the HiRes images is about $1.9' \times 1.1'$, a significant improvement over the $\sim 4' \times 3'$ beam in pre-HiRes images. The biggest advantage of having beam-matched maps in all four bands, however, is to make infrared color maps that would be physically meaningful. One can then easily compare colors of different regions, provided that the sizes of regions over which the flux integrations are made is larger than the beam size.

COMPARISON WITH OTHER OBSERVATIONS

Before trying to interpret the physical meaning of the HiRes images and color maps, it is necessary to assess the reliability of the enhanced features seen in the HiRes deconvolution. In IC 443, this can be best shown in comparisons with observations of the same region made in other wavelengths.

Using millimeter-wave radio telescopes, Dickman et. al. (1992, see also Huang et. al. 1986) mapped the broad CO and HCO+ line emission in the surrounding areas of IC 443. These molecular lines, typically as broad as 60 km s^{-1}, are often identified as the shock interface with nearby molecular clouds. Overlapping the CO and HCO+ maps with the deconvolved IRAS images, we find that all broad molecular line regions also have strong FIR emission. These regions are located mainly along the ω-shaped ring structure in the middle and southern parts of the SNR. Some of the previously unresolved FIR features, such as the one corresponding to "position F" (Dickman et. al. 1992) near the geometric center of IC 443, are clearly isolated FIR emission peaks, similar to their counterparts in the molecular line survey.

Burton et. al. (1988, 1993) made extensive maps of the (1–0) S(1) line emission of molecular hydrogen covering the entire region of IC 443. The near-infrared line represents shocked molecular gas at a warm ($\sim$ 2000 K) temperature. Although the H_2 map is at a much higher resolution, the overall correspondence with the deconvolved IRAS images is striking. This suggests that the mid- and far-infrared emission detected by IRAS is mainly from heated dust associated with the shocked molecular gas traced by the H_2 line emission. This comparison serves two purposes: on the one hand, some emission regions with structures poorly resolved in the HiRes images can be studied by referring to the NIR image; conversely, the FIR color information extracted from comparing different IRAS bands can be used to help interpret the significant variations of H_2 emission around this SNR (see below).

Wang et. al. (1994) mapped the 21 cm neutral hydrogen line emission of IC 443 with relatively high resolution (15″ as compared to the 50″ resolution in previous studies). Again, the regions with strong infrared and molecular line emission also show up prominently with broad-line H I. Detailed comparisons indicate that the detected H I is mainly the diffuse gas resulting from shock dissociation of molecules as the SNR interacts with the surrounding dense clouds. However, the kinematic information from HI is incomplete due to the foreground

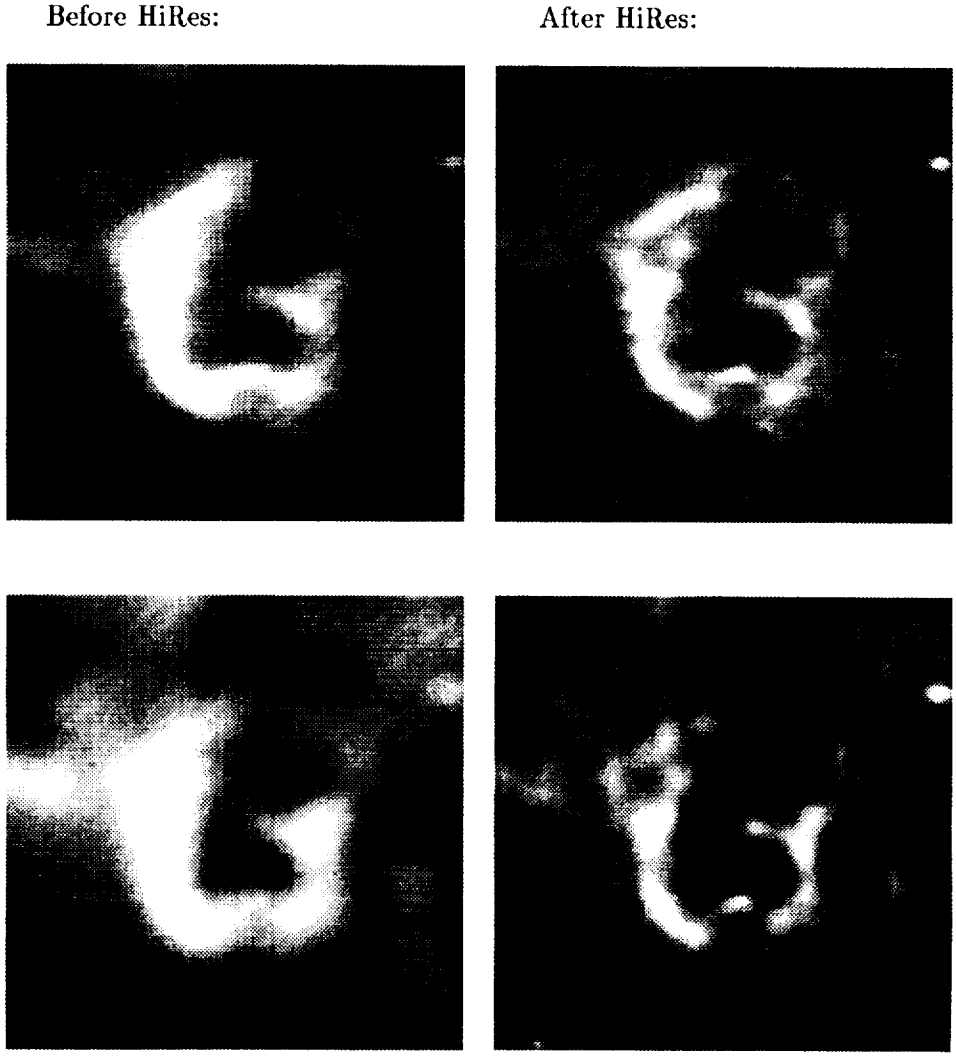

FIGURE 1 Greyscale maps of the IRAS 60 (upper) and 100 μm (lower) images of IC 443 before and after HiRes processing. This is a one-degree field centered on the supernova remnant; north is at top, and east is to the left. Grey levels are linear. Some of the vertical stripes seen in the processed images are due to artifacts of the deconvolution algorithm. The HiRes images are "beam matched", such that the effective resolutions are very similar (see text).

absorption within the Galactic plane.

Finally, the IPC aboard Einstein and, more recently, the PSPC aboard ROSAT both made large-scale diffuse X-ray emission maps of IC 443 in the 0.1–3 KeV energy range (Petre et. al. 1988; Rho & Petre 1993). Comparison between the infrared and soft X-ray maps is intriguing because the higher energy photons are emitted by the hot interior of the SNR bubble (e.g., Arendt et. al. 1991). Indeed, their positional coincidence with the rim of X-ray emitting regions provides independent confirmation that much of the faint structures seen in the HiRes images, especially in the NW region of IC 443, are actual SNR shock fronts.

In summary, the HiRes images with much improved resolution clearly demonstrate the relationship between the mid- and far-infrared emission and the SNR shock interactions in the ISM.

INFRARED COLOR VARIATION

As pointed out above, one of the great advantages for having beam-matched IRAS images is to construct color maps of infrared emission, which are important to the studies of shock interactions.

In the case of IC 443, we find that the FIR color changes drastically from one part of the SNR shell to the other, presumably tracing the density variation in the ambient medium. In the NE part of the SNR where the optical filaments are prominent, there is a low S(12)/S(25) and a high S(60)/S(100) flux density ratio as compared to the rest of the FIR bright regions (SE and SW), where molecular line emissions are the strongest.

Theoretically, the energy spectrum of the dust emission in interstellar shocks depends critically on the average preshock density, n_0. Where n_0 is low, the shock speed is high and so is the heating rate. The corresponding FIR (60 and 100 μm) color then reflects a higher dust temperature. Conversely, lower dust temperatures are found where the preshock density is high. In IC 443, the latter case is typically regions dominated by molecular gas.

We have also obtained spectroscopic (echelle) data of the optical filaments at a velocity resolution of about 8 km s^{-1}. Since the curvature of the shock front always tends to broaden the observed linewidth, it can be shown that the FWHP (full-width at zero power) of the emission lines of any particular region is a direct indicator of the shock speed at that position. And it is so regardless of the actual angle between the shock velocity vector and the line of sight (Dopita 1979). Adopting this assumption, we find in the NE where the S(60)/S(100) color ratio is high, the shock speed is about twice that of the SE and SW regions (120 km s^{-1} versus 60 km s^{-1}). The optical data thus confirm the idea that the SNR has encountered very dense gas in the southern part, resulting in faster cooling and a dramatic slow-down in the shock propagation.

The detailed morphology of the regions with different FIR colors can also be quite different. Referring to the high resolution H_2 line images, we find that the NE region shows thin, multi-layered filamentary structures; while the SE and SW regions show more pronounced, ripple-like features (Burton et. al. 1993). These difference could be due to the changing characteristics of the shock as its speed drops substantially (e.g., Wang & Scoville 1992).

DISCUSSION

One other thing that is clear from the color maps is that an enhanced ratio of S(60)/S(100) is usually accompanied by a decreased S(12)/S(25). This is also true for integrated fluxes of a large sample of SNRs (e.g., Arendt 1989). It reminds one of a similar trend among galaxies (Helou 1986), which is accounted for in terms of changing conditions in the ionizing radiation (Désert 1986). In the case of SNR shocks, however, the explanation maybe somewhat different. It is likely that the color ratio change among different shocked regions in a SNR is directly related to the amount of very small grains (VSG) that survive at the shock front. Faster shocks in the diffuse gas (with warmer 60–100 μm emission) tend to destroy most of the VSGs which are responsible for the emission at the shortest (12 μm) wavelength, resulting in a lower S(12)/S(25) ratio.

For interstellar shocks in dense gas, line emissions could potentially alter the colors measured using IRAS flux density ratios. Burton et. al. (1990) detected a strong [OI]λ 63 μm line at one of the molecular emission peaks in IC 443, and estimated that it may contribute substantially to the local broad-band 60 μm flux density. If this is generally the case, then the IRAS data, even with the beam-matched images, cannot be used to derive effective dust temperatures directly. More FIR spectroscopic observations are therefore needed to help better address the real properties of dust emission in the shocked ISM.

ACKNOWLEDGMENTS

I thank the staff at IPAC for providing technical support for the HiRes processing, and I am grateful to Dr. M. G. Burton for his help in analyzing the data discussed in this contribution. This work was carried out in part at the Jet Propulsion Laboratory, California Institute of Technology, under a contract with the National Aeronautics and Space Administration.

REFERENCES

Arendt, R.G. 1989, *Ap. J. Suppl. Ser.*, **70**, 182

Arendt, R.G., Dwek, E., & Petre, R. 1991, *ApJ*, **368**, 474

Aumann, H.H., Fowler, J.W., & Melnyk, M. 1990, *A.J.*, **99**, 1674

Braun, R. & Strom, R. 1986, *A&A*, **164**, 193

Burton, M.G., Geballe, T.R., Brand, P.W.J. T., & Webster, A.S. 1988, *MNRAS*, **231**, 617

Burton, M.G., Hollenbach, D.J., Hass, M.R., & Erickson, E.F. 1990, *ApJ*, **355**, 197

Burton, M.G., Spyromilio, J. & Wang, Z. 1993, *in preparation*

Désert 1986, F.X., in *Light on Dark Matter*, ed. F.P. Israel, 213

Dickman, R.L., Snell, R.L., Ziurys, L.M., & Huang, Y.L., 1992, *ApJ*, **400**, 203

Dopita, M. 1979, *Ap. J. Suppl. Ser.*, **40**, 455

Helou, G. 1986, *Ap.J. Lett.*, **311**, L33

Huang, Y.L., Dickman, R.L., & Snell, R.L. 1986, *ApJ*, **302**, L63

Petre, R., Szymkowiak, A.E., Seward, F.D., & Willingale, R. 1988, *ApJ*, **335**, 215

Rho, J. & Petre, R. 1993, in *IAU Colloq. 145: Supernova and Supernova Remnants*, eds. R. McCray and Z.R. Wang (Cambridge), *in press*

Saken, J.M., Fesen, R.A., & Shull, M. 1992, *Ap.J. Suppl. Ser.*, **81**, 715

Wang, Z. & Scoville, N.Z. 1992, *apj*, **386**, 158

Wang, Z., Scoville, N.Z., Burton, M.G., & Kenney, J.P. 1994, *in preparation*